Combustion Chemistry

Hai Wang
Stanford University
2015 Princeton-CEFRC Summer School On Combustion
**Course Length: 3 hrs**
June 22 – 26, 2015

Lecture 6

6. Homogeneous Reacting Flows without Transport Influence

In this lecture we will provide a background of theory and practice of simple chemically reacting flow simulations. We shall focus on homogeneous reactors in which the fluid transport and mixing is unimportant. In general, chemical reaction models developed in these simulations are later used for more complex flow conditions, including laminar diffusion flames or turbulent premixed and diffusion flames.

6.1 Types of Reacting Flows

There are several important aspects that are used to classify chemically reacting flows. Under the no-flow condition, the reaction is characterized purely by a time evolution of species concentration with known initial conditions of premixed fuel, oxidizer and diluent mixtures. Most of the practical combustion problems involve fluid flow and mixing. Reacting flows or flames are often categorized depending on whether the fuel and oxidizer are premixed or non-premixed. In addition, reacting flows may be classified depending on whether the flow is laminar or turbulent. Here we shall not discuss turbulent reacting flows.

Perhaps the most important consideration in reacting flow simulation is the degree and type of fluid mixing. The mixing can occur among the reactants or between reactants and products. Traditionally reaction models are developed from experiments in which fluid mixing and thus its uncertainty is completely suppressed. Research reactors of this type include shock tubes, turbulent flow reactors, and rapid compression machines (see, Figure 6.1). In these reactors, the reaction is expected to be homogeneous. In other words, there is no mixing among the reactants and among reactants and products.
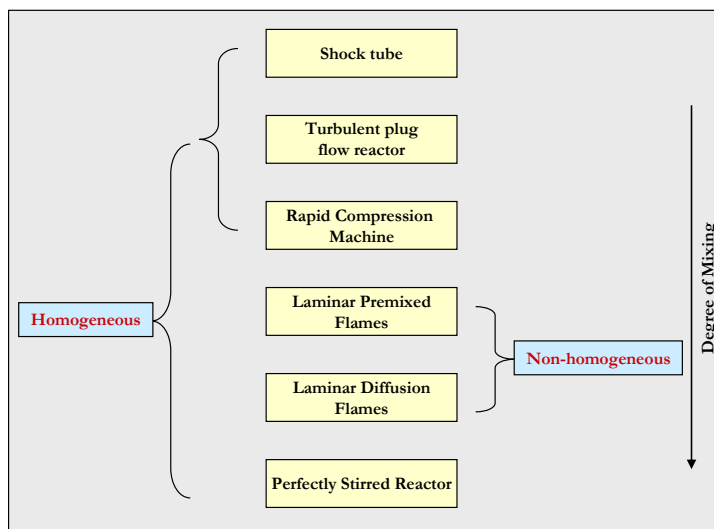
Figure 6.1 Summary of typical research reactors

In general, flames always involve some mixing and require a consideration of transport phenomena along with reaction kinetics. In laminar premixed flames, for example, mixing occurs because of species diffusion. Laminar diffusion flames, on the other hand, mixing of

the fuel and oxidizer by molecular diffusion is a necessity. Excessive mixing can also generate homogeneous reaction condition. That is, if the reactor is "stirred," leading to time scales of mixing between the reactants and products far shorter than the chemical time scales, the reactor may be approximated as a perfectly stirred reactor or continuously stirred tank reactor.

In this lecture, we shall learn the theory and application of simulation methods for homogeneous reacting flows. We shall briefly discuss the principle and application of several research reactors.
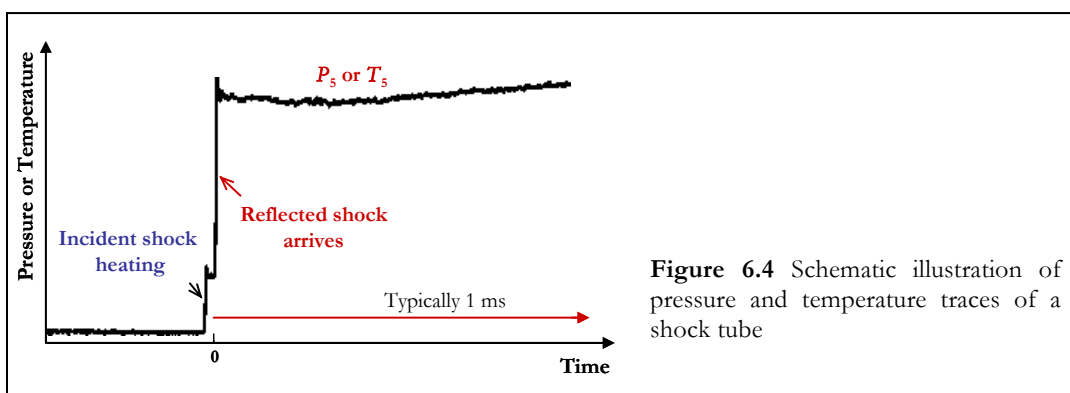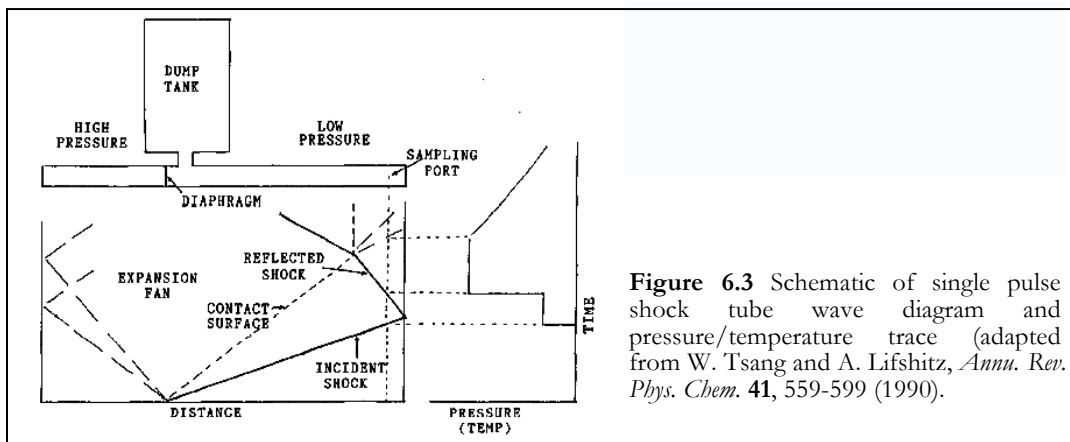
6.2 Shock Tubes
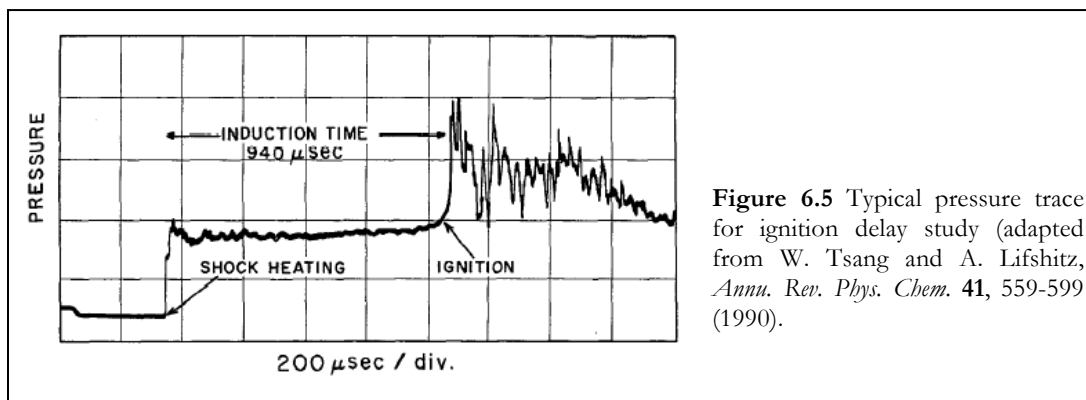
6.2.1 Principle of Design and Operations

A simple shock tube is made of a metal tube separated by a diaphragm into two sections (see, Figure 6.2): the driver section in which an inert gas at high pressure and a driven section hosting a reacting gas at low pressures. Upon sudden burst of the diaphragm, a shock wave is generated, which travels rapidly into the driven section and instantly heats up the reactant gas (See, Figure 6.3). This shock wave is known as the incident shock. The pressure and temperature in a gas heated by incident shock wave are often referred to as P_2 and T_2. If the end section of the driven section is a flat surface, the incident shock wave reaching the end surface is reflected into already heated gas, resulting in a further rise in the temperature (T_5) and pressure (P_5). The result is almost instantaneous heating of the reactant mixture as seen in Figure 6.4, allowing chemical reactions to be studied from a well define time zero under a nearly fixed initial temperature and pressure. Depending on shock tube designs, typical accessible ranges of pressure and temperature are 0.1 to 500 atm and 800 to 3000 K, respective. The reaction time is typically up to 2 ms.
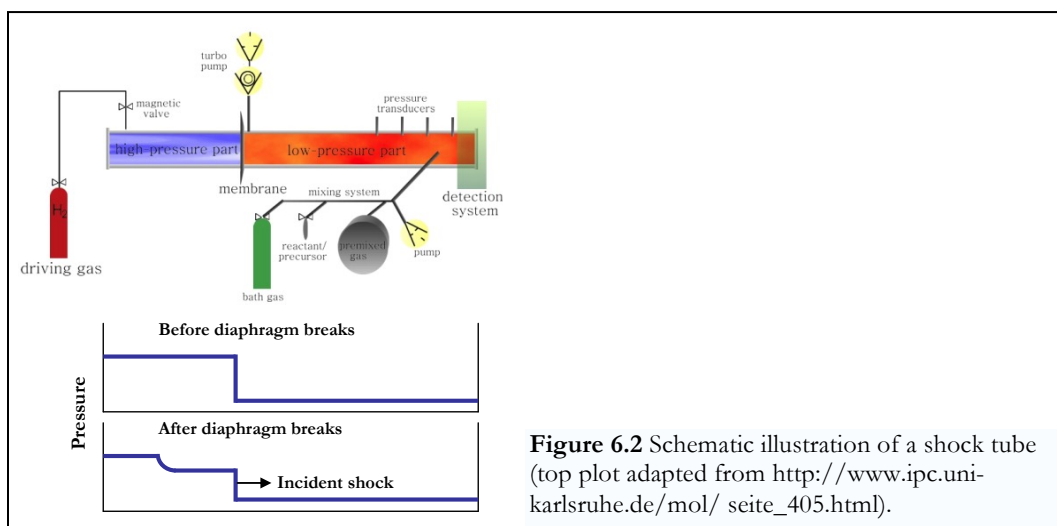
Figure 6.2 Schematic illustration of a shock tube (top plot adapted from http://www.ipc.uni-karlsruhe.de/mol/ seite_405.html).

Figure 6.3 Schematic of single pulse shock tube wave diagram and pressure/temperature trace (adapted from W. Tsang and A. Lifshitz, *Annu. Rev. Phys. Chem.* **41**, 559-599 (1990).

Figure 6.4 Schematic illustration of pressure and temperature traces of a shock tube

There are numerous experimental methods that have been utilized to analyze the reaction processes in a shock tube. The simplest measurement is the continuous monitoring of the pressure trace. If a fuel-oxygen-inert mixture undergoes ignition, the rapid heat release causes a sudden increase in temperature and pressure after a period of time (see, Figure 6.5). The time from the beginning of shock heating and the onset of pressure rise is called the *induction time* of ignition or *ignition delay*. The ignition delay may be measured also by the onset of light emission.

Figure 6.5 Typical pressure trace for ignition delay study (adapted from W. Tsang and A. Lifshitz, *Annu. Rev. Phys. Chem.* **41**, 559-599 (1990).

The reaction progress may also be monitored by a variety of laser absorption experiments. In these experiments, the concentrations of one or several intermediate species (e.g., $OH\bullet$ and $CH_3\bullet$) may be measured as a function of time. Depending on the shock tube design, the reaction may be quenched by the arrival of the contact surface separating the driver and driven gas (see, Figure 6.3). The resulting reacted gas may then be analyzed for the extent of reaction and concentrations of reactants, and reaction intermediates and products, by mass spectrometry or gas chromatography.

6.2.2 Shock Tube Simulation

Because the transport time scale is usually longer than a few milliseconds, the reaction inside a shock tube is adiabatic and homogeneous without interference of fluid transport and heat loss. Experiments behind reflected shock wave may be simulated purely as an initial value problem. The species conservation equation describing the time evolution of K species in I elementary reactions is given by

$$\frac{dy_k}{dt} = \frac{\dot{\omega}_k W_k}{\rho} \quad \left(k=1,...,K\right) , \tag{6.1}$$

where y_k is the mass fraction of species k, $\dot{\omega}_k$ is its molar production rate, W_k is the molecular weight, and ρ is the mixture mass density. Under the adiabatic, constant-volume/density condition, the conservation of energy requires that

$$\rho c_v \frac{dT}{dt} + \sum_{k=1}^{K} \bar{u}_k \dot{\omega}_k W_k = 0 , \tag{6.2}$$

where $\bar{u}_k$ is the total internal energy

$$\bar{u}_k = \bar{h}_{T,k} - R_u T , \tag{6.3}$$

$\bar{h}_{T,k}$ is the total enthalpy of species k (see, equations 1.25b and 1.60). The equation of state is given by the ideal gas law,

$$P = \frac{\rho R_u T}{\bar{W}} , \tag{6.4}$$

where $\bar{W}$ is the mean molecular weight of the mixture,

$$\bar{W} = \sum_{k=1}^{K} x_k W_k , \tag{6.5}$$

and x_k is the mole fraction.

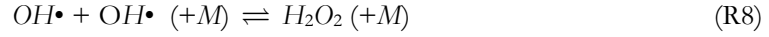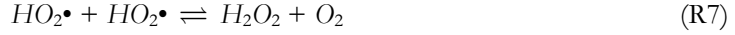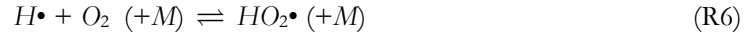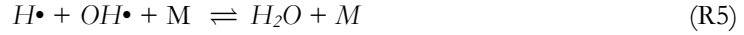In equation (6.2), the molar production rate is given by

$$\dot{\omega}_k = \sum_{i=1}^{I}\left(\nu''_{k,i} - \nu'_{k,i}\right)\left\{k_{f,i}\prod_{l=1}^{K}\left[A_l\right]^{\nu'_{k,i}} - \frac{k_{f,i}}{K_{c,i}}\prod_{l=1}^{K}\left[A_l\right]^{\nu''_{k,i}}\right\}, \qquad (6.6)$$

for a generalized reaction model written as

$$\sum_{k=1}^{K}\nu'_{k,i}A_k \rightleftharpoons \sum_{k=1}^{K}\nu''_{k,i}A_k \quad \left(i=1,...,I\right), \qquad (6.7)$$

where A_k is the kth chemical species, $\nu'_{k,i}$ and $\nu''_{k,i}$ are the stoichiometric coefficients of the kth species in the ith reaction, $k_{f,i}$ and $K_{c,i}$ are the forward rate coefficient and the equilibrium constant of the ith reaction, respectively.

The compact notation of a reaction model (equation 6.7) may be illustrated by examining the simplified model of hydrogen oxidation as an example,

$$H_2 + O_2 \rightleftharpoons H\bullet + HO_2\bullet \qquad (R1)$$
$$H\bullet + O_2 \rightleftharpoons OH\bullet + O\bullet \qquad (R2)$$
$$O\bullet + H_2 \rightleftharpoons OH\bullet + H\bullet \qquad (R3)$$
$$OH\bullet + H_2 \rightleftharpoons H_2O + H\bullet \qquad (R4)$$
$$H\bullet + OH\bullet + M \rightleftharpoons H_2O + M \qquad (R5)$$
$$H\bullet + O_2 \ (+M) \rightleftharpoons HO_2\bullet \ (+M) \qquad (R6)$$
$$HO_2\bullet + HO_2\bullet \rightleftharpoons H_2O_2 + O_2 \qquad (R7)$$
$$OH\bullet + OH\bullet \ (+M) \rightleftharpoons H_2O_2 \ (+M) \qquad (R8)$$

Here we have a total of $K = 9$ species (H_2, O_2, H_2O, $H\bullet$, $O\bullet$, $OH\bullet$, $HO_2\bullet$, H_2O_2, and N_2) and $I = 8$ reactions. Therefore the stoichiometric coefficient matrixes are

|				ν'									ν''					
					i									i				
	k	1	2	3	4	5	6	7	8	1	2	3	4	5	6	7	8
H_2	1	1	0	1	1	0	0	0	0	0	0	0	0	0	0	0	0
O_2	2	1	1	0	0	0	1	0	0	0	0	0	0	0	0	1	0
H_2O	3	0	0	0	0	0	0	0	0	0	0	0	1	1	0	0	0
$H\bullet$	4	0	1	0	0	1	1	0	0	1	0	1	1	0	0	0	0
$O\bullet$	5	0	0	1	0	0	0	0	0	0	1	0	0	0	0	0	0
$OH\bullet$	6	0	0	0	1	1	0	0	2	0	1	1	0	0	0	0	0
$HO_2\bullet$	7	0	0	0	0	0	0	2	0	1	0	0	0	0	1	0	0
H_2O_2	8	0	0	0	0	0	0	0	0	0	0	0	0	0	0	1	1
N_2 or Ar	9	0	0	0	0	0	0	0	0	0	0	0	0	0	0	0	0

In realistic combustion modeling, the reaction model employed is usually quite large. The full reaction model shown in Figure 3.7 for hydrogen and carbon monoxide oxidation contains 13 species and 30 elementary chemical reactions. Typical reaction models of methane oxidation at high temperatures contain about 30 chemical species and 150 reactions. For more complex hydrocarbon fuels, the size of the reaction model increases very rapidly as the fuel size increases.

If the reaction is carried out under the constant-pressure condition, the governing equations are similar. The equation of energy conservation, however, becomes

$$\rho c_p \frac{dT}{dt} + \sum_{k=1}^{K} \bar{h}_{T,k} \dot{\omega}_k W_k = 0 \ . \tag{6.8}$$

In general, shock tube experiments without significant heat release during the course of reaction may be simulated as a constant-pressure process, whereas those with significant heat release should be simulated as a constant volume/density process. Figure 6.6 shows the difference of the pressure and temperature traces obtained with the constant-volume and constant-pressure simulations ($20\%H_2$-$10\%O_2$-$70\%Ar$, P_5 = 0.54 atm, T_5 = 1400 K). Despite the difference seem in the final temperature, the time delay to the onset of reaction is predicted to be about the same. This type of simulation allows the computed ignition delay time τ, as seen in Figure 6.6, to be compared with the experimental data (see, Figure 6.7). In doing so, we may examine the validity of a proposed reaction model.

It is also possible to carry out direct comparison of the time evolution of a particular species concentration. For example, Figure 6.8 shows the experimental and computed mole fraction profiles of $CH_3\bullet$ produced from shock heating a CH_4-O_2-Ar mixture at 2225 K and 1 atm. This type of comparison is very useful, in that it provides a more stringent check of a reaction model for its ability to predict the onset of reaction as well as the intricate reaction kinetics that occurs after the onset of reaction.
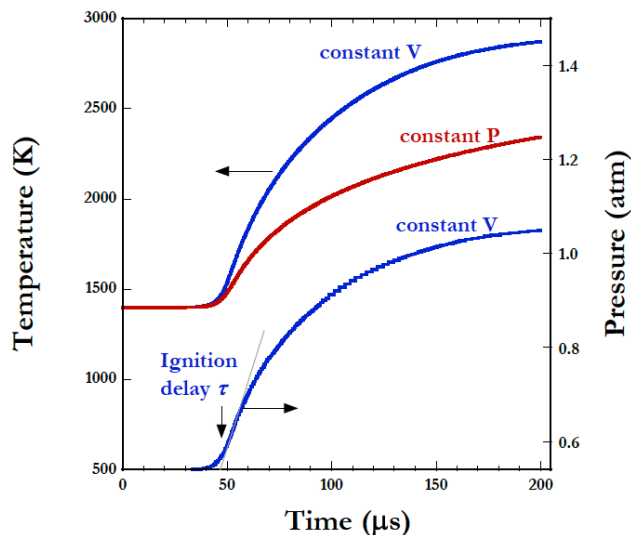
Figure 6.6 Temperature and pressure traces computed for $20\%H_2$-$10\%O_2$-$70\%Ar$, P_5 = 0.54 atm, T_5 = 1400 K, using the reaction mechanism of Davis, S. G., Joshi, A. V., Wang, H., and Egolfopoulos, F., "An optimized kinetic model of H_2/CO combustion." *Proceedings of the Combustion Institute*, **30**, pp. 1283-1292, 2005 (see, Figure 3.7).
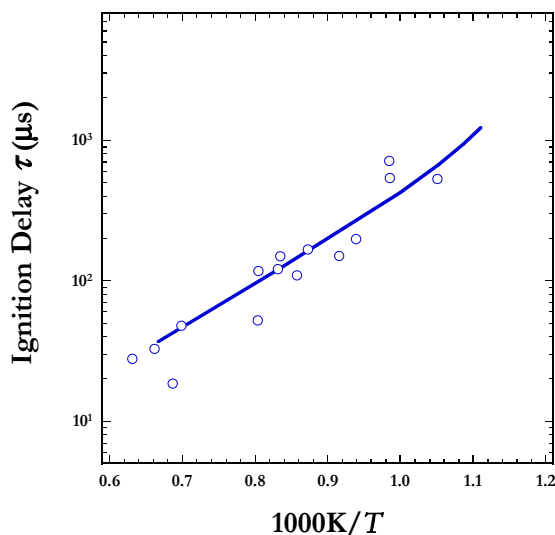
Figure 6.7 Experimental[*] (symbols) and computed (line) ignition delay times for $20\%H_2$-$10\%O_2$-$70\%Ar$, $P_5 = 0.54$ atm as a function of T_5. The computation used the reaction model of Davis et al. (see Figure 6.6 caption).
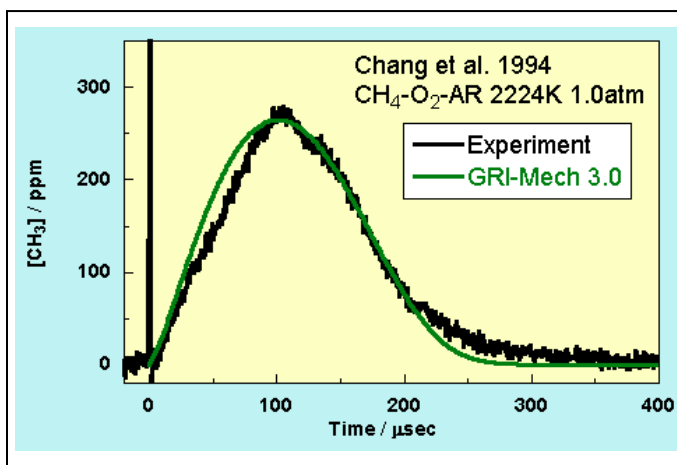
Figure 6.8 Experimental[†] (symbols) and computed (line) mole fraction profile of CH3• produced from shock heating of 994ppm CH_4 + 2021ppm O_2 + Ar at 2224K and 1 atm (taken from http://www.me.berkeley.edu/gri_mech/version30/text30.html#performance).

6.3 Turbulent Flow Reactors

A turbulent flow reactor is usually made of a quartz tube imbedded in insulation materials or a tubular heat to maintain nearly adiabatic or isothermal condition. The reactant is rapidly mixed with a hot dilute gas in the mixing section and injected into the test section. As the gas flows down the tube, the reaction time is essentially given by the length from the injector divided by the convective velocity. The highly turbulent condition virtually eliminates the boundary layer that develops near the wall of reactor tube, and in doing so leads to the plug flow condition. The ranges of pressure and temperature accessible to flow reactor are 1 to

---
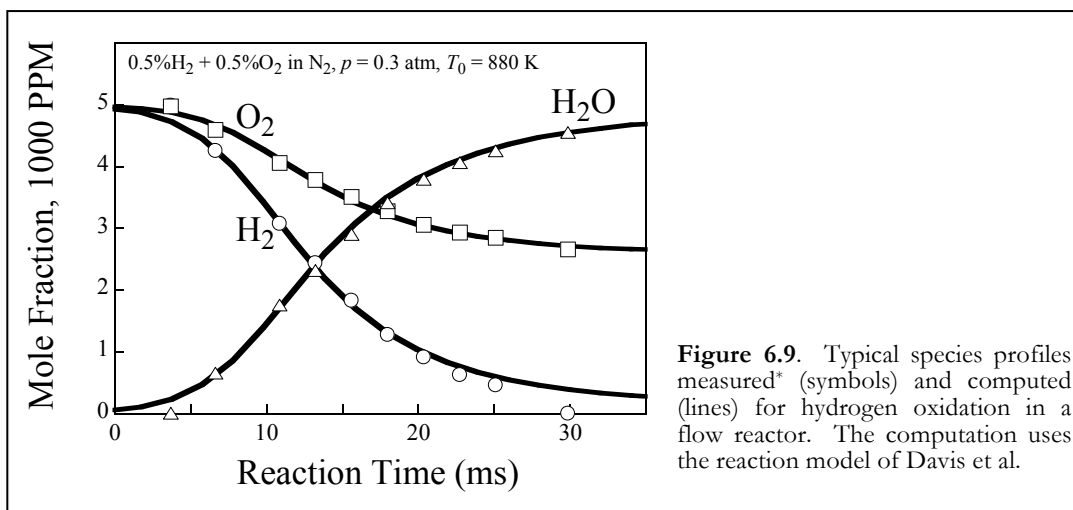
[*] Cohen, A. and Larsen J., Report BRL 1386, (1967).

[†] Chang, A.Y., Davidson, D.F., DiRosa, M., Hanson, R.K., and Bowman, C.T., Shock Tube Experiments for Development and Validation of Kinetic Models of Hydrocarbon Oxidation, Work-in-Progress Poster 3-23, 25th Combustion Symposium

100 atm and 700 to 1400 K, respectively. The reaction time is usually of the order of tens to hundreds of milliseconds.

Gas sampling is usually accomplished with a cooled sampling probe inserted from the end of the reactor. Depending on the position of the probe, species concentration may be measured as a function of the distance from the reactant injector or the reaction time. Figure 6.9 shows the time evolution of reactants H_2 and O_2 and product H_2O as a function of reaction time. Notice that in this case the reactants are highly diluted, so the violent combustion reaction is replaced by slow and gentle oxidation of hydrogen into water, which provide a very good time resolution to achieve accurate measurements.

The simulation of flow reactant experiments uses the governing equations same as those for shock tube simulation. Because the pressure is constant in the flow tube, the equation of energy conservation under the constant-pressure condition is employed. Figure 6.9 shows the comparison of experimental and computed species concentration profiles.

The graph is labeled: Mole Fraction, 1000 PPM (y-axis); Reaction Time (ms) (x-axis); $0.5\%H_2 + 0.5\%O_2$ in N_2, $p = 0.3$ atm, $T_0 = 880$ K; curves labeled O_2, H_2, H_2O.

Figure 6.9. Typical species profiles measured[*] (symbols) and computed (lines) for hydrogen oxidation in a flow reactor. The computation uses the reaction model of Davis et al.

6.4 Perfectly Stirred Reactor

Perfectly stirred reactor (PSR) is an approximation of such experimental reactors as the jet stirred reactor or continuously stirred tank reactor. Unlike the turbulent, plug flow reactor, a jet stirred reactor is designed to achieve complete mixing of the reactants and products. This is often accomplished by the gas in the reaction vessel continuously stirred by the entering, highly turbulent reactant feed jets, thus trying to produce uniform or nearly uniform condition in the reactor. While the reaction condition is far less defined compared to the shock tube and turbulent flow reactor, the jet stirred reactor has the advantage that the role of fluid mixing on reaction kinetics may be studied in the limit of fast mixing.

---

[*] M. A. Mueller, R. A. Yetter, F. L. Dryer, *Int. J. Chem. Kinet.* 31 (1999) 705-724.

The species and energy conservation equations for an adiabatic PSR may be written respectively in the transient form as follows,

$$\frac{dy_k}{dt} = \frac{y_{k,0} - y_k}{\tau} + \frac{\dot{\omega}_k W_k}{\rho} \ , \tag{6.9}$$

$$\bar{c}_p \frac{dT}{dt} = \frac{1}{\tau} \sum_{k=1}^{K} y_{k,0} \left(h_{T,k,0} - h_{T,k} \right) - \frac{\sum_{k=1}^{K} \bar{h}_{T,k} \dot{\omega}_k W_k}{\rho} \ , \tag{6.10}$$

where the subscript "0" denotes the reactant condition, τ is the mean residence time,

$$\tau = \frac{\rho V}{\dot{m}} \ , \tag{6.11}$$

V is the reactor volume, and $\dot{m}$ is the mass flow rate. Under the steady state, both equations (6.9) and (6.10) are set to be equal to zero, the mass flow rate of entering gas is equal to the mass rate of the out flow.

6.5 Reaction Mechanism Compilation

The simulation of all reactors considered above requires a detailed reaction model and a thermochemical database. The thermochemical database has been discussed in Lecture 1. Here we shall focus on the reaction model.

A reaction model is a collection of elementary reactions and their associated rate coefficients. The reaction model should not only be a qualitative description of the reaction mechanism through which the fuel is oxidized, it should also quantitatively predict such important properties as the heat release rate, the rate of fuel disappearance and product formation, and even the concentrations of intermediate species. A sample hydrogen and carbon monoxide reaction model has been discussed in Lecture 3 (Figure 3.7).

Compilation of a reaction model is a tedious task. Fortunately, there have been a large number of published reaction models that may be viewed and downloaded from

http://www.reactiondesign.com/support/open/datalinks.html

In addition, comprehensive and careful rate coefficient evaluations have been sporadically made over the last two decades. See, for example,

Baulch. D. L., Bowman, C. T., Cobos, C. J., Cos, R. A., Just, T., Kerr, J. A., Pilling, M. J., Stocker, D., Troe, J., Tsang, W., Walker, R. W., Warnatz, J. "Evaluated kinetic data for combustion modeling: Supplement II" *Journal of Physical and Chemical Reference data* 34, 757-1397 (2005).

Baulch, D. L., Cobos, C. J., Cox, R. A., Frank, P., Hayman, G., Just, T., Kerr, J. A., Murrells, T., Pilling, M. J., Troe, J., Walker, R. W., and Warnatz, J. "Evaluated kinetic data for combustion modeling: Supplement I" *Journal of Physical and Chemical Reference data* **23**, 847-1033 (1994).

Baulch, D. L., Cobos, C. J., Cox, R. A., Esser, C., Frank, P., Just, T., Kerr, J. A., Pilling, M. J., Troe, J., Walker, R. W., and Warnatz, J. "CEC group on evaluation of kinetic data for combustion modeling," *Journal of Physical and Chemical Reference Data* **21**, 411-734 (1992).

Tsang, W. and Hampson, R. F. "Chemical kinetic database for combustion chemistry .1. methane and related-compounds," *Journal of Physical and Chemical Reference Data* **15**, 1087-1279 (1986).

Tsang, W. "Chemical kinetic database for combustion chemistry .2. Methanol," *Journal of Physical and Chemical Reference Data* **16**, 471-508 (1987).

Tsang, W. "Chemical kinetic database for combustion chemistry .3. Propane," *Journal of Physical and Chemical Reference Data* **17**, 887-952 (1988).

6.6 Rate Coefficient Evaluation

Here we illustrate how a rate coefficient expression is evaluated. We shall use the important combustion reaction

$$CO + OH\bullet \rightarrow CO_2 + H\bullet, \tag{6.12}$$

as an example. We shall denote the rate coefficient of (6.12) as k_{ca}. Figure 6.10 shows selected experimental data for

$$CO + OH\bullet \rightarrow products. \tag{6.13}$$

Since the reaction is classically known as a chemically activated reaction, we expect k_{ca} to be pressure dependent, since it is the sum of reaction (6.12) and reaction (6.14),

$$CO + OH\bullet \rightarrow HOCO\bullet. \tag{6.14}$$

At the very low pressure, the rate coefficient of (6.14) is negligibly small; the rate coefficient of (6.12) is independent of pressure. That is, from equation (5.85) the rate coefficient of the chemically activated reaction becomes

$$\lim_{P \to 0} k_{ca} = K_c \int_{E_{0,1}}^{\infty} \frac{k_2(E) k_{1b}(E) P_{AB}(E) dE}{k_{1b}(E) + k_2(E)}, \tag{6.15}$$

which is independent of pressure, and from equation (5.85) the rate for the bimolecular combination reaction is

$$\lim_{P \to 0} k_{bi} = \beta \omega K_c \int_{E_{0,1}}^{\infty} \frac{k_{1b}(E) P_{AB}(E) dE}{k_{1b}(E) + k_2(E)} \to 0. \tag{6.16}$$

It follows that the sum of rate coefficients of (6.12) and (6.14) is independent of pressure at the low-pressure limit. As the pressure is increased,

Indeed the experimental data presented in Figure 6.10 shows that at very low pressure (e.g., P = 1 Torr), the total rate coefficient collapse onto a single curve. The data depicted by the $P \to 0$ curve must be the rate coefficient of reaction (6.12). At the atmospheric pressure (P = 1 Bar), the rate coefficient starts to deviate from the low-pressure limit below ~600 K, where the bimolecular combination (6.14) becomes dominant. The data of Figure 6.10 also show that at elevated pressure (P = 10 and 100 Bar), reaction (6.14) can become important at high temperatures.

We may now consider some more experimental data collected at fairly low pressure or specifically for reaction (6.12), as shown in Figure 6.11. The peculiar k-versus-T dependence could not be fitted with a traditional modified Arrhenius expression. Rather, it may be shown that a bi-Arrhenius expression of Davis et al.[7] (the solid line in Figure 6.11)

$$k\left(\mathrm{cm^3 mol^{-1} s^{-1}}\right) = 1.33 \times 10^{-12} T^{0.14} e^{-3700/T} + 1.46 \times 10^{-13} T^{0.03} e^{8/T},$$
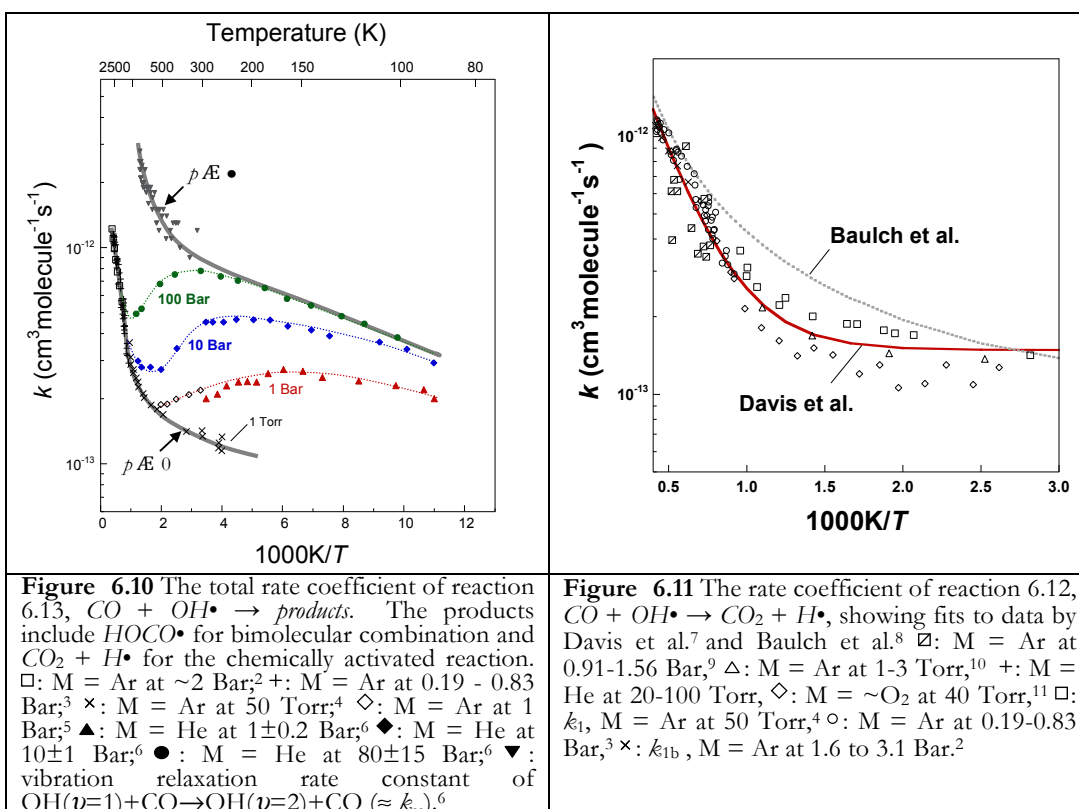
represents the data in the entire range of temperature much better than the traditional modified Arrhenius expression of Baulch et al.[8] (the dotted line in Figure 6.11). A recent theoretical treatment of the reaction (6.14) supports this bi-Arrhenius expression[1] (see attached supplemental reading).

The above discussion suggests that to properly interpret rate coefficient data, one need to have a basic knowledge of reaction rate theories introduced in Lectures 4 and 5. In fact, the above bi-Arrhenius expression is critical to the prediction of laminar flame speeds of CO, H_2 and air mixtures.

We remark that this type of rate evaluation makes it possible to compile an accurate and physically justified reaction mechanism, such as the one shown in Figure 3.7.

---

[1] Joshi, A. V. and Wang, H. "Master equation modeling of wide temperature and pressure dependence of CO + OH → products." *International Journal of Chemical Kinetics*, in press, 2005.

Figure 6.10 The total rate coefficient of reaction 6.13, $CO + OH\bullet \rightarrow$ *products*. The products include $HOCO\bullet$ for bimolecular combination and $CO_2 + H\bullet$ for the chemically activated reaction. □: M = Ar at ~2 Bar;[2] +: M = Ar at 0.19 - 0.83 Bar;[3] ×: M = Ar at 50 Torr;[4] ◇: M = Ar at 1 Bar;[5] ▲: M = He at 1±0.2 Bar;[6] ◆: M = He at 10±1 Bar;[6] ● : M = He at 80±15 Bar;[6] ▼: vibration relaxation rate constant of $OH(\upsilon{=}1){+}CO{\rightarrow}OH(\upsilon{=}2){+}CO$ ($\approx k_\infty$).[6]

Figure 6.11 The rate coefficient of reaction 6.12, $CO + OH\bullet \rightarrow CO_2 + H\bullet$, showing fits to data by Davis et al.[7] and Baulch et al.[8] ☑: M = Ar at 0.91-1.56 Bar,[9] △: M = Ar at 1-3 Torr,[10] +: M = He at 20-100 Torr,[11] ◇: M = ~O_2 at 40 Torr,[11] □: k_1, M = Ar at 50 Torr,[4] ○: M = Ar at 0.19-0.83 Bar,[3] ×: k_{1b}, M = Ar at 1.6 to 3.1 Bar.[2]

[2] Golden, D. M.; Smith, G. P.; McEwen, A. B.; Yu, C. L.; Eiteneer, B.; Frenklach, M.; Vaghjiani, G. L.; Ravishankara, A. R.; Tully, F. P. J Phys Chem A 1998, 102, 8598-8606.

[3] Wooldridge, M. S.; Hanson, R. K.; Bowman, C. T. Int J Chem Kinet 1994, 26, 389-401.

[4] Ravishankara, A. R.; Thompson, R. L. Chem Phys Lett 1983, 99, 377-381.

[5] Jonah, C. D.; Mulac, W. A.; Zelinski, P. J Phys Chem 1984, 88, 4100-4104; Beno, M. F.; Jonah, C. D.; Mulac, W. A. Int J Chem Kinet 1985, 17, 1091-1101.

[6] Fulle, D.; Hamann, H. F.; Hippler, H,; Troe, J. J Chem Phys 1996, 105, 983-1000.

[7] Davis, S. G., Joshi, A. V., Wang, H., and Egolfopoulos, F., "An optimized kinetic model of H_2/CO combustion." *Proceedings of the Combustion Institute*, **30**, pp. 1283-1292, 2005.

[8] Baulch, D. L., Cobos, C. J., Cox, R. A., Esser, C., Frank, P., Just, T., Kerr, J. A., Pilling, M. J., Troe, J., Walker, R. W., and Warnatz, J. "CEC group on evaluation of kinetic data for combustion modeling," *Journal of Physical and Chemical Reference Data* **21**, 411-734 (1992).

[9] Brabbs, T.A.; Belles, F.E.; Brokaw, R.S. in Thirteenth Symposium (International) on Combustion, The Combustion Institute, Pittsburgh, PA, 1971, p. 129.

[10] Westenberg, A. A.; deHaas, N. J. J Chem Phys 1973, 58, 4061-4065.

[11] Vandooren, J.; Peeters, J.; Van Tiggelen, P.J. in Fifteenth Symposium (International) on Combustion, The Combustion Institute, Pittsburg, PA, 1975, p. 745